JGR Space Physics

RESEARCH ARTICLE
10.1029/2022JA030385

Occurrence Statistics of Horse Collar Aurora

G. E. Bower[1], S. E. Milan[1,2], L. J. Paxton[3], and B. J. Anderson[3]

[1]School of Physics and Astronomy, University of Leicester, Leicester, UK, [2]Birkeland Centre for Space Science, Bergen, Norway, [3]Johns Hopkins University Applied Physics Laboratory, Laurel, MD, USA

Key Points:

- Horse collar aurora, teardrop shaped polar cap, occur frequently approximately 8 times per month and are linked to dual lobe reconnection
- Interplanetary magnetic field B_x does not appear to be an important factor in determining the occurrence of horse collar aurora
- The dawn arc of the horse collar auroras is usually brighter than the dusk

Correspondence to:

G. E. Bower,
geb21@leicester.ac.uk

Citation:

Bower, G. E., Milan, S. E., Paxton, L. J., & Anderson, B. J. (2022). Occurrence statistics of horse collar aurora. *Journal of Geophysical Research: Space Physics*, *127*, e2022JA030385. https://doi.org/10.1029/2022JA030385

Received 14 FEB 2022
Accepted 11 MAY 2022

Abstract Horse collar aurora (HCA) are an auroral feature where the dawn and dusk sector auroral oval moves polewards and the polar cap becomes teardrop shaped. They form during prolonged periods of northward interplanetary magnetic field (IMF), when the IMF clock angle is small. Their formation has been linked to dual-lobe reconnection (DLR) closing magnetic flux at the dayside magnetopause. The conditions necessary for DLR are currently not well-understood therefore understanding HCA statistics will allow DLR to be studied in more detail. We have identified over 600 HCA events between 2010 and 2016 in UV images captured by the Special Sensor Ultraviolet Spectrographic Imager instrument on-board the Defense Meteorological Satellite Program spacecraft F16, F17 and F18. As expected, there is a clear preference for HCA occurring during northward IMF. We find no clear seasonal dependence in their occurrence, with an average of 8 HCA events per month. The occurrence of HCA events does not appear to depend on the B_x component of the IMF. Considering the average radiance intensity across the dusk-dawn meridian shows the HCA as a separate bulge inside the auroral oval and that the dawn side arc of the HCA is usually brighter than the dusk in the Lyman-Birge-Hopfield short band. We relate this to the expected field aligned current pattern of HCA formation. We further suggest that transpolar arcs observed in the dawn sector simultaneously in both northern and southern hemispheres are misidentified HCA.

Plain Language Summary Horse collar auroras (HCA) form when the auroras move to high latitudes at dawn and dusk. They have been proposed to be formed by a process called dual-lobe reconnection, which takes place when the interplanetary magnetic field (IMF) embedded in the solar wind is directed almost exactly northwards. We study the occurrence of HCA in auroral observations from the Special Sensor Ultraviolet Spectrographic Imager instrument onboard satellites of the Defense Meteorological Satellite Program for the years 2010 to 2016. Studying the occurrence of HCA and the solar wind conditions under which they form allows us to gain new insights into the conditions necessary for dual-lobe reconnection (DLR) to occur which are currently not well-understood. We find that there are approximately 8 HCA events per month, with no seasonal dependence, and that the IMF must be within 30 degrees of northwards. When looked at by season no variation is seen in the IMF B_x component therefore suggesting that B_x is not an important factor in the occurrence of HCA. We also note a dawn-dusk asymmetry in the brightness of the HCAs, which we attribute to the polarity of the field-aligned electrical currents which produce the auroras.

1. Introduction

Horse collar aurora (HCA) is an auroral phenomenon that occurs during northward IMF, named due to the shape of the emitting area. They consist of two arcs and a region of soft particle precipitation called 'web' which contain weak (sometimes subvisual) aurora (Hones et al., 1989). It has been suggested that small-scale Sun-aligned arcs and HCA are closely related to each other. The polar cap arcs that occur most frequently are those that occur in the morning or evening sectors of the polar cap (Hosokawa et al., 2020) and these may constitute the web. In one reported event from 6th January 2013 space-based optical observations from the SSUSI (Special Sensor Ultraviolet Spectrographic Imager) instrument on board a Defense Meteorological Satellite Program (DMSP) satellite show an HCA configuration, while simultaneous ground-based 630.0 nm observations from an all-sky imager at Resolute Bay, Canada, show the morning web of the HCA to be formed of a number of small-scale sun aligned arcs (Hosokawa et al., 2020).

Hones et al. (1989) suggested that the HCA may move in relation to changes in IMF B_y. In their observation from DE 1 auroral images of the southern hemisphere on 9th May 1983 they show the evolution of an HCA from its start time of 08:23 UT until around 10:35 UT. During this period the IMF B_z was about +5 nT and the B_y component was negative before 09:20 UT when it changed to positive. The centroid of the polar slot (the dim region

poleward of the HCA, which we identify with the polar cap) moved from dusk to dawn and it was suggested that this movement could be linked to the IMF B_y change.

In a preliminary estimate of the frequency of occurrence of HCA, Hones et al. (1989) found that HCA occur approximately one third of the time during quiet geomagnetic conditions. This was based on September–November 1981 DE 1 observations with 83 very quiet condition sequences. In 35% of these HCA were identified. In another 35% there may have been HCA but low light level and poor viewing conditions made it impossible to make a positive identification. 16% of images did not have HCA and theta auroras occurred in 12 of the 83 sequences.

Meng (1981) suggested a mechanism for the formation of the HCA by a poleward expansion of the auroral oval on the dusk and dawn side during northward IMF, with the expansion of the oval relating to either the thickening or tilting of the central plasma sheet. If the central plasma sheet thickens on the dawnside this could lead to a poleward expansion of the auroral oval as the morning web of the HCA. If this thickening of the plasma sheet occurred on the dawn and dusk sides simultaneously then there would be poleward expansion of the auroral oval on both sides leading to an HCA configuration. MHD simulations by Tanaka et al. (2017) were able to produce signatures of small-scale Sun-aligned arcs in field-aligned current (FAC) distributions on both sides of the polar cap forming an HCA configuration with significant thickening of the plasma sheet seen on both sides (Hosokawa et al., 2020).

Milan et al. (2020) proposed that the HCA is produced by dual-lobe reconnection closing magnetic flux at the dayside magnetopause. This causes a contraction of the polar cap, observed as a poleward motion of the dawn and dusk open/closed field line boundary (OCB) to form the characteristic teardrop shape observed during HCA. Ionospheric flows are observed to be sunwards out of the noon-sector polar cap and antisunwards within the regions of HCA. This results in flow shears at the poleward edges of the HCA, requiring field-aligned currents (FACs) which are upwards at dawn and downwards at dusk. Milan et al. (2020) suggested that these FACs, especially the upwards FAC at dawn, are expected to be related to the occurrence of auroral emissions along the poleward edge of the HCAs.

The conditions necessary for dual-lobe reconnection to occur are not well-understood at present. Lobe reconnection is thought to occur when the IMF is directed northwards, such that the fields either side of the lobe magnetopause are antiparallel. If the IMF has a significant B_y component then the reconnection sites in the northern and southern hemispheres will be displaced from noon, and reconnection in the two hemispheres will take place with different IMF field lines. This is referred to as single lobe reconnection (an IMF field line reconnects with a single lobe), though can occur simultaneously in both hemispheres. However, the rate of reconnection in the two hemispheres could be different, perhaps because the summer hemisphere may be preferred for reconnection, and/or the polarity of the IMF B_x component could favor the antiparallel condition in the north or the south. Dual-lobe reconnection, leading to the closure of magnetospheric flux, is thought to occur when B_y is near-zero (that is, the clock angle is near-zero) such that the same IMF field line reconnects in both the north and the south. Imber et al. (2006) estimated that the absolute value of the clock angle had to be less than 10° for DLR to occur. However, it might be expected that seasonal and B_x component factors could also affect its occurrence, maybe leading to SLR rather than DLR even for near-zero clock angle.

These issues have been hard to investigate due to the difficulty of identifying when DLR is actually taking place. However, if the formation of HCAs can be used as a proxy for the occurrence of DLR, then studies of northward IMF reconnection geometries are facilitated. The aim of the present paper is to determine occurrences of HCA over a seven year interval, and to use these to better understand the conditions that favor DLR.

The present paper follows on from a previous study of the occurrence of transpolar arcs (TPAs) in DMSP/SSUSI data (Bower et al., 2022). A discussion of the observing biases of the DMSP spacecraft with season and UT can be found it that report. In addition, in common with previous studies, (Fear & Milan, 2012; Hosokawa et al., 2011; Rairden & Mende, 1989; Valladares et al., 1994), Bower et al. (2022) found a preponderance of TPAs in the dawn sector in both the northern and southern hemispheres. In most cases TPAs appear at dawn in the northern (southern) hemisphere and dusk in the southern (northern) hemisphere if IMF B_y is negative (positive). However, there are many cases in which TPAs appear at dawn in both hemispheres. In this present study we investigate whether these dawn-dawn cases are actually mis-identified HCAs.

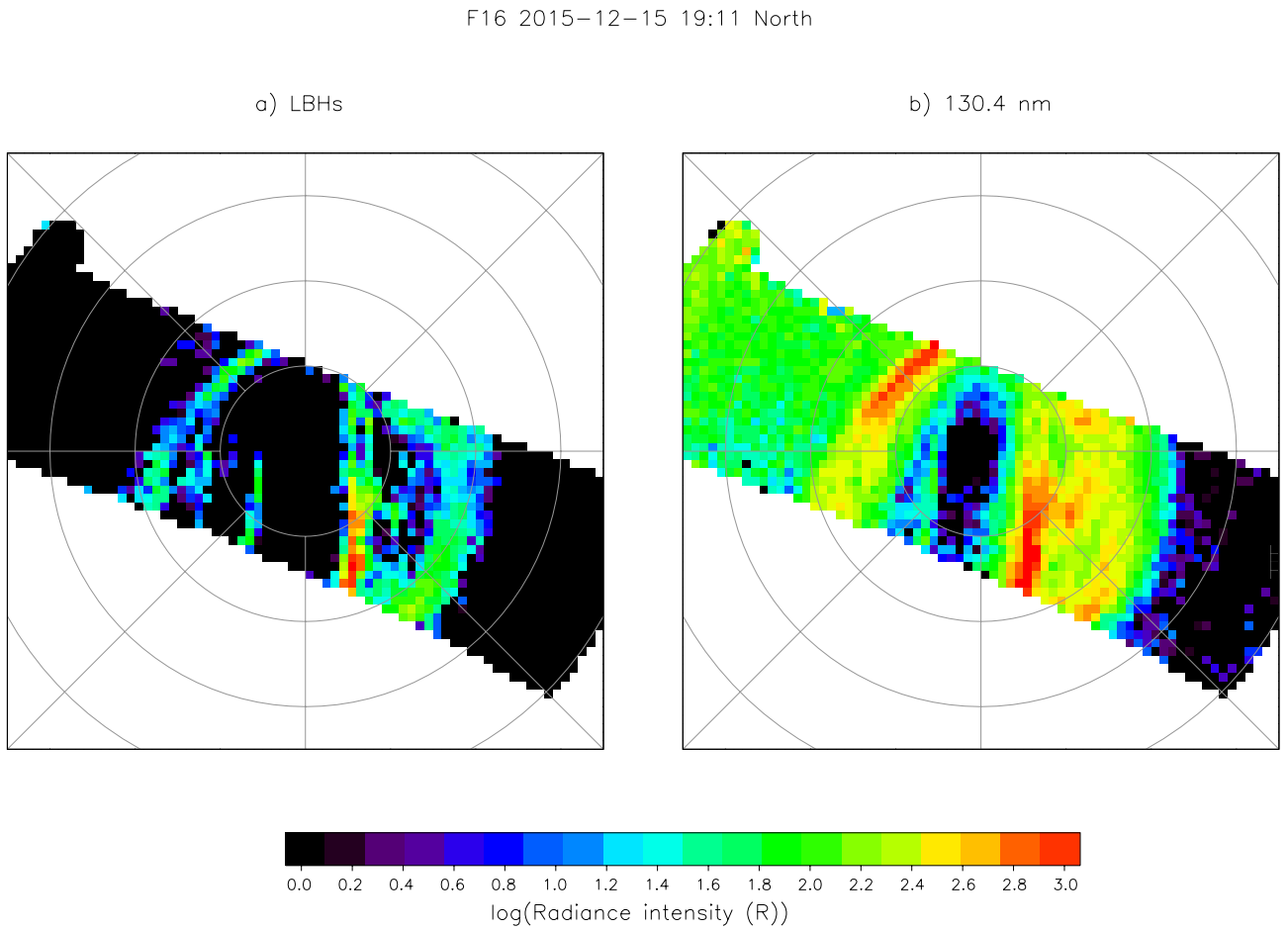

Figure 1. Example of HCA identified in the DMSP/SSUSI data on 15th December 2015 at 19:11 UT in the northern hemisphere. (a) LBHs (b) 130.4 nm.

In this paper, we study the occurrence statistics of HCA. Section 2 describes the instrumentation used in the study along with the HCA occurrence statistics (Section 2.1) and associated IMF conditions (Section 2.2). Section 2.3 focusses on the average radiance intensity of the HCA events across the dusk-dawn meridian. The results are discussed in Section 3. Section 3.2 focuses on conjugate TPAs identified by the detection algorithm in Bower et al. (2022), in particular those which appear to form at dawn in both hemispheres which we relate to HCA. Finally, Section 4 concludes.

2. Observations

The data used is from the Special Sensor Ultraviolet Spectrographic Imager (SSUSI) instrument on board Defense Meteorological Satellite Program (DMSP) spacecraft F16, F17 and F18 which were all operational between 2010 and 2016 thus providing near-simultaneous inter-hemispheric observations (Paxton et al., 1992, 1993, 2017). The SSUSI instrument builds up images of the auroral emission in the polar region by scanning antisunward from its roughly dawn-dusk orbit over approximately 20 min, and of each hemisphere approximately every 50 min as they are in 101.6 minute sun-synchronous orbits with an altitude of 833 km (nominal). The DMSP/SSUSI data was visually inspected to identify horse collar aurora (HCA). An example of an HCA in the DMSP/SSUSI data is shown in Figure 1. HCA were identified when there is aurora seen at high latitudes in the polar regions on both sides on the midnight meridian. SSUSI obtains the entire FUV spectrum. Due to data rate limitations five spectral segments or 'colors' are downlinked in imaging mode (Paxton et al., 1992). Only Lyman-Birge-Hopfield short band (LBHs) and 130 nm wavelength were used to identify the HCA. These wavelengths were chosen as they are usually the clearest in the DMSP/SSUSI data, with 135.6 nm and Lyman-Birge-Hopfield long band (LBHl)

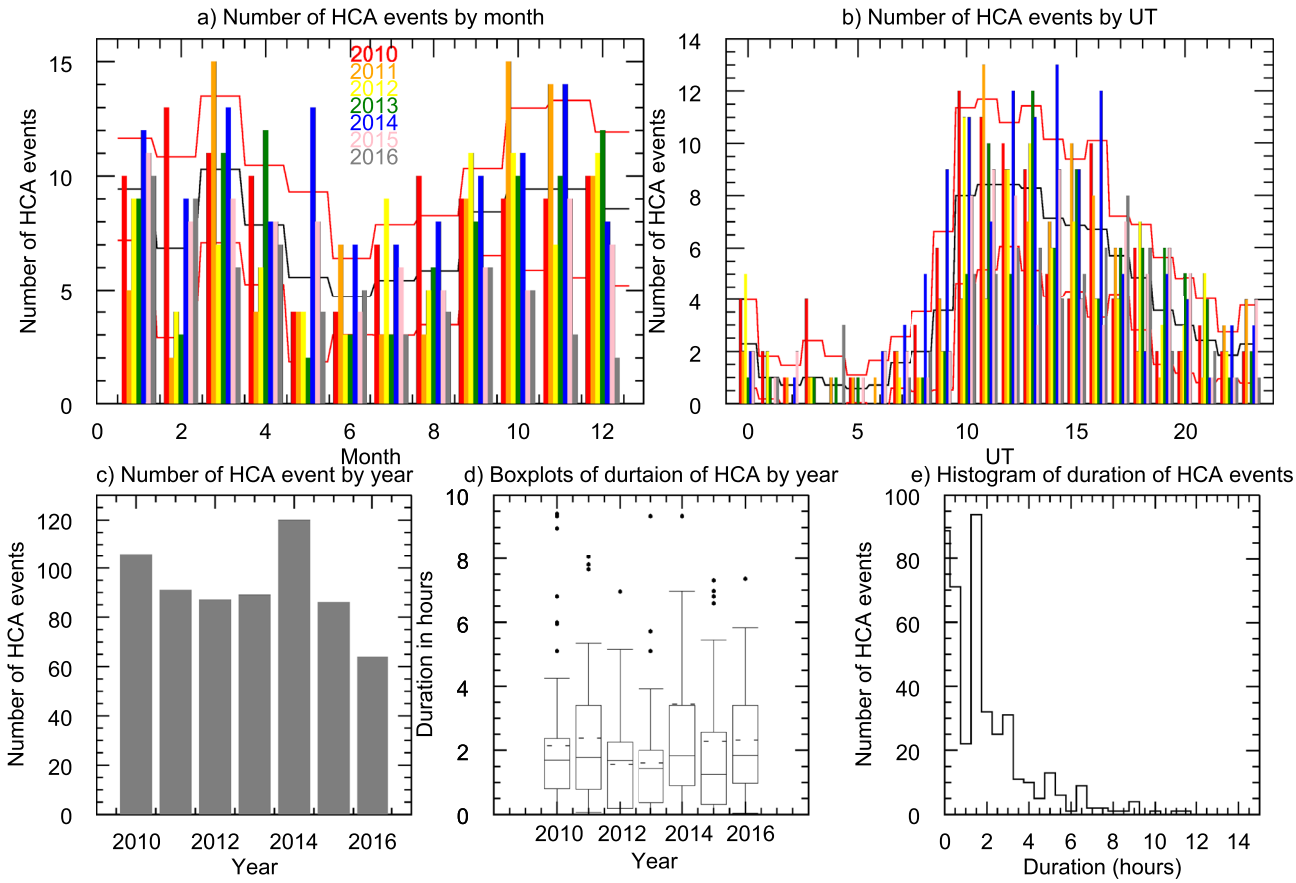

Figure 2. (a) Number of HCA events identified by year and month. (b) Number of HCA events identified by year and UT. The black line is the mean of each month and the red the standard deviation. (c) Number of HCA events identified by year. (d) Boxplots of the duration in hours of the HCA events made up of multiple DMSP/SSUSI image. The dotted line is the mean. (e) Histogram of the duration of the HCA events in 30 minute bins.

being the next clearest. Lyman alpha is usually the least clear in comparison to the other wavelengths because the ubiquitous geocoronal H Lyman-alpha emission is often far brighter than the auroral signal.

2.1. HCA Occurrence

Over the seven years analyzed, 642 HCA events were identified, of which 435 were multiple DMSP/SSUSI image events (when the HCA was observed in two or more consecutive passes of either hemisphere) and 207 were single DMSP/SSUSI image events. Figure 2a shows the distribution of HCA by month for each year, the black line is the mean value for each month and the red lines show plus and minus one standard deviation. There are an average of 8 HCA events per month. There is no clear signature of a seasonal dependence, though perhaps a dip in occurrence in the months June and July. We tested the significance of this by performing a chi-squared test on the average distribution (black line) and found a p-value of 0.9218 therefore the null hypothesis of a uniform distribution is not rejected. Figure 2b is in the same format as Figure 2a but for the UT distribution. As discussed by Bower et al. (2022) the orbits of the DMSP spacecraft introduce a viewing bias into the observations by SSUSI. This distribution here is consistent with the viewing bias modeled by Bower et al. (2022) and as such we suggest that the true occurrence of HCA by time-of-day is uniform.

Figure 2c shows the number of HCA identified each year: on average there are approximately 90 HCA events per year. The data were collected from near the end of the extended solar minimum of SC23 (2010) until near the minimum at the end of SC24 (2016). No dependence on average F10.7 index is seen. The duration of the 435 HCA events made up of multiple DMSP/SSUSI images is approximated using the first and last DMSP/SSUSI image as the start and end times respectively. Boxplots of the duration of the HCA events by year are shown in Figure 2d which shows that there is not much variation in duration of the HCA events by year with a mean

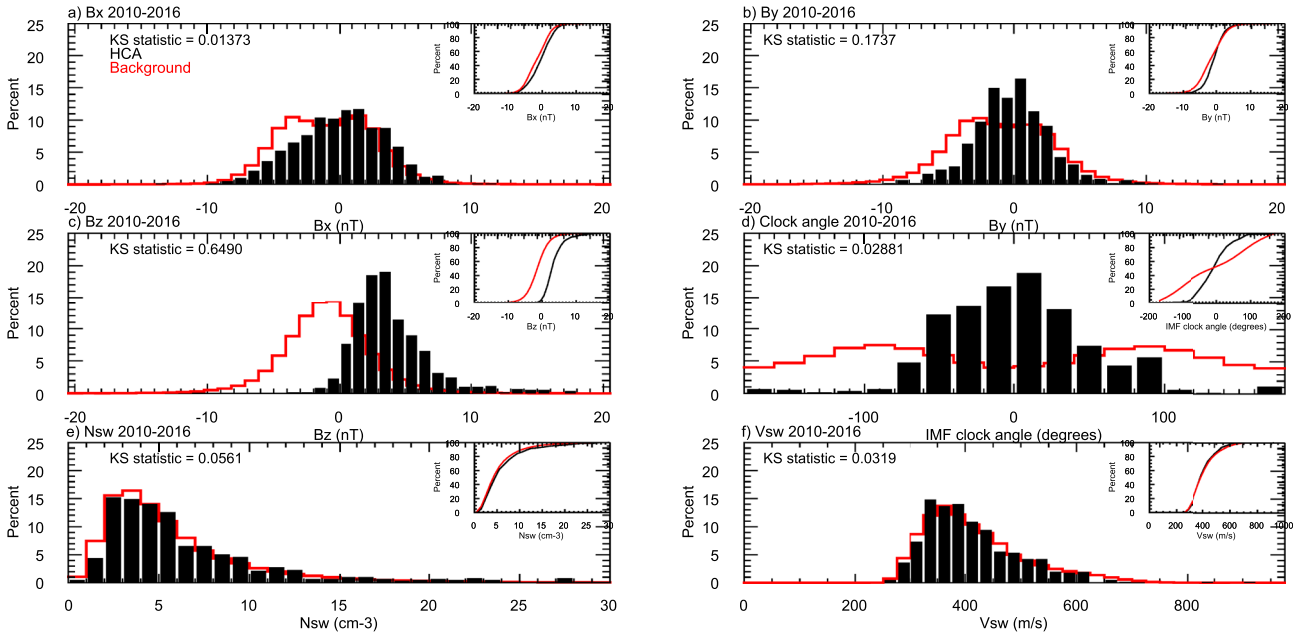

Figure 3. IMF data for black) HCA and red) background (a) B_x (b) B_y (c) B_z (d) IMF clock angle,θ (e) Solar wind density (f) Solar wind speed. The top right of each panel is the CDF used in KS test.

duration of 2.29 hr Figure 2e shows the number of HCA events by duration in 30 bins and shows that the majority of the HCA events have a duration of less than 2 hr. Due to the data gaps and limited spatial coverage at certain UTs of the DMSP/SSUSI data it is difficult to pinpoint the exact start and end times of the HCA event, as the HCA may have formed before the first image and/or persist afterward.

2.2. IMF Conditions

The solar wind and IMF conditions were considered for the hour before the HCA event (Figure 3). The IMF data used is from the OMNI data set with 1 minute cadence (King & Papitashvili, 2005). The red curves in Figure 3 show the background distributions, the average solar wind and IMF conditions between 2010 and 2016. The black is the IMF conditions averaged over the hour before the time of the first HCA image in each event. Percentages are used to make the two curves comparable. We note that the average IMF clock angle is found from the average of the components. The B_x, B_y, solar wind density and solar wind speed components (Figures 3a, 3b, 3e, and 3f respectively) all follow the same pattern for the HCA events as for the non HCA times. Only IMF B_z and IMF clock angle, θ (Figures 3c and 3d respectively) have a clear departure from the background distribution, such that the HCA form when the IMF B_z is positive and θ is small.

There is perhaps a slight preference for IMF B_y conditions near zero (Figure 3b) but it is not significant based on a Kolmogorov–Smirnov (KS) test, the results of which are shown in the upper right corner of each panel in Figure 3, the inset panel are the cumulative distribution functions (cdfs) used for the KS test. Only θ and B_z (Figures 3c and 3d respectively) have KS test statistics greater than the critical threshold (0.2302) to accept the null hypothesis with a significance level of 0.01.

If the occurrence of dual-lobe reconnection (and hence HCA) was dependent on IMF Bx, any seasonal variation in the occurrence of HCA could be explained by the variation in dipole tilt. We investigated whether this could produce the dip in HCA events in June and July. Figure 4a shows the average IMF B_x distribution in the hour before the HCA event for the northern hemisphere summer solstice (May, June and July) in red and winter solstice (November, December and January) in blue. From this it can be seen there is no clear difference in the distributions. However in Figure 4b we show the distributions for the equinoxes, spring equinox (February, March and April) in yellow and the autumn equinox (August, September and October) in green, and in this case there does appear to be a difference. This is supported by the KS test results shown in the upper left corner of the plots. During the spring equinox months the HCA appear occur more often when B_x is negative and during the autumn

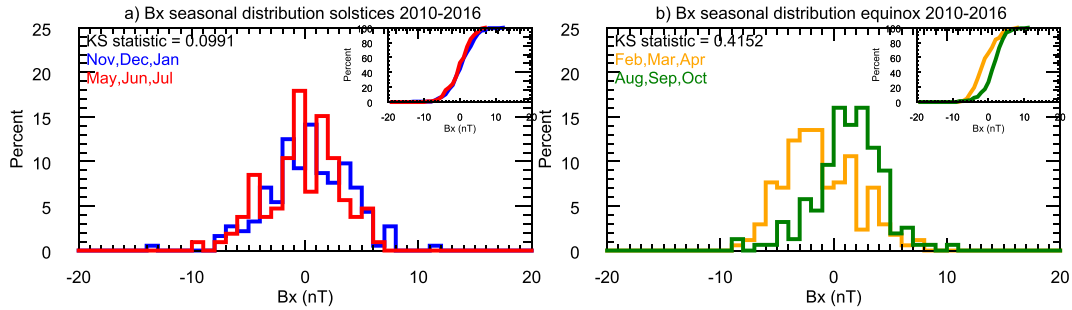

Figure 4. Number of HCA events in nT bins of the average B_x component in the hour before the start of the HCA event (a) solstices (b) equinoxes. red) May, June and July blue) November, December and January green) August, September and October yellow) February, March and April. The top right of each panel is the CDF used in KS test.

equinox they occur more often under positive B_x however this is likely due to the GSM coordinate system used as discussed in Section 3.1.

Figure 5a shows how the average θ varies in hour bins before the first image in each HCA event, from 0-1 hour to 3–4 hr before the event. Average θ was calculated from the average B_y and B_z components during the hour bin with periods of no data removed. From this it is clear that θ reduces as the start time of the HCA approaches. For each of the distributions we calculated the mean resultant length, R, which is a measure of the concentration of the data in a particular direction (Mardia & Jupp, 2009). The values of R for the hour bins are shown in the top right of each panel in Figure 5a. A value of $R = 1$ means that the distribution is concentrated in one direction bin only. R increased as the start time of the HCA approaches, from 0.32 in the 3–4 hr before to 0.77 in the hour before. In the hour before the HCA event the clock angle reduces to between −33° and 25° for 50% of the events.

The length of time that θ stays below 20° in the hours before the HCA event is also considered. Figure 5b shows boxplots of how long θ is between 20 and -20° in the 4 hr before the start of the HCA event, with the mean value plotted as the dotted line. From this, it is clear that the absolute value of θ is less than 20° for longer as the start time of the HCA approaches, with it reaching a mean of 9.4 min in the hour before the HCA event.

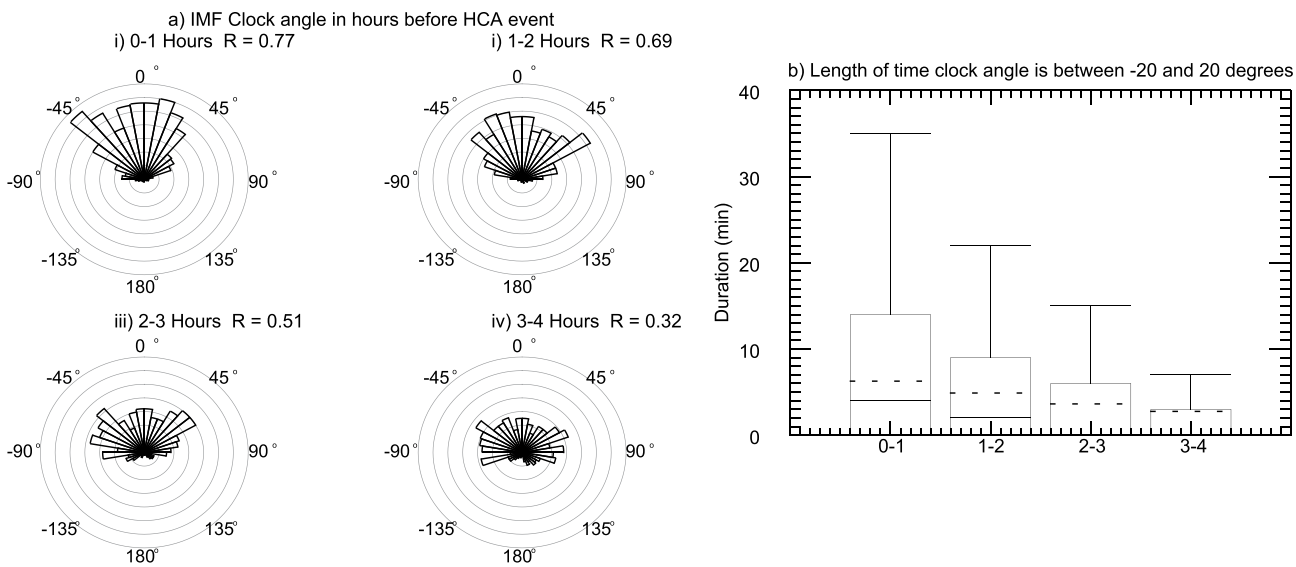

Figure 5. (a) IMF Clock angle for the 4 hr before the HCA first image. (b) Boxplots of the duration of time that the IMF stays below 20° in the hours before the first HCA image in an event.

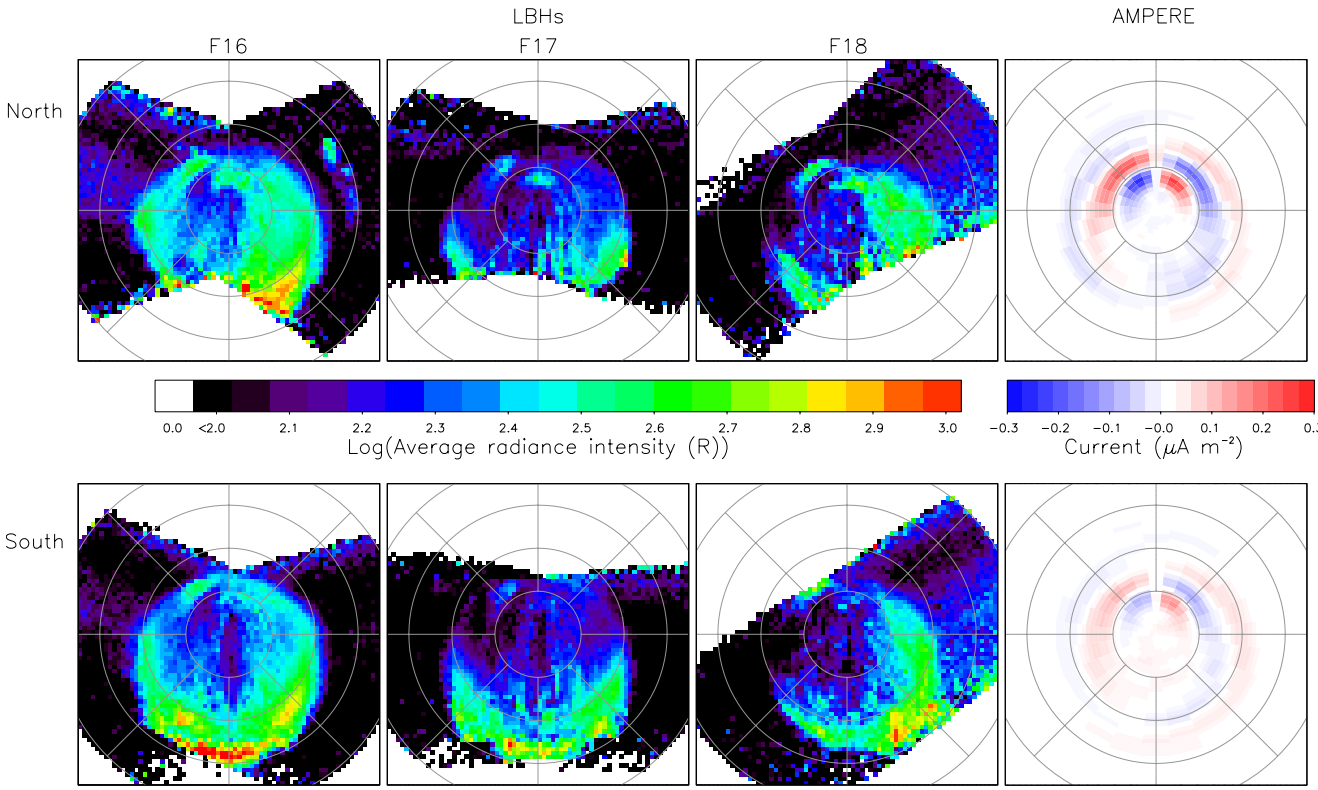

Figure 6. The average radiance intensity LBHs DMSP/SSUSI image for the HCA event and Average AMPERE current map for the HCA events. Top row of each panel is northern hemisphere and bottom southern hemisphere. From left to right the columns are F16, F17, F18 and average AMPERE current map for the HCA events.

2.3. Average Radiance Intensity

We now investigate the average pattern of auroral radiance observed during the HCA events. The average radiance of the LBHs DMSP/SSUSI images for the HCA events are broken down by spacecraft and hemisphere and presented in Figure 6. The same figure has been created for the other SSUSI wavelengths but is not shown. The top and bottom rows are northern and southern hemispheres, respectively. These were created by stacking the DMSP/SSUSI images and taking the average. The HCA appears as auroral emission poleward of the main auroral oval, especially at dawn and dusk. The HCA appears clearer in the F16 data particularly for LBHl, LBHs and 130.4 nm. It is interesting to note that the three spacecraft appear to identify different features. F16 identified more clearly the auroral web of the HCA. F17 and F18 identify bright spots that are located pre-noon poleward of 80° latitude, and post-noon (15 MLT) equatorward of 80° latitude which are co-located with expected upward current described by Milan et al. (2022). The auroras producing the pre-noon spot are referred to by previous works as High Latitude Detached Arcs (HiLDAs), and are produced by the NBZ (northward B_Z) reverse convection pattern and the associated upward field aligned currents (Carter et al., 2018; Frey, 2007; Paxton & Zhang, 2016).

The right-most panel of Figure 6 shows the average field-aligned current density for the HCA events. The top plot is for the northern hemisphere and the bottom is the southern hemisphere. These measurements are provided by the Active Magnetosphere and Planetary Electrodynamics Response Experiment (AMPERE) with data available between 2010 and 2016 approximately every 10 min. It does this by using the magnetic perturbations measured by the 66 satellites that make up the Iridium telecommunication network. These satellites are in 6 polar orbital planes at an altitude of 780 km thus a 104 min orbit period (Anderson et al., 2000; Coxon et al., 2018; Waters et al., 2001).

As expected the average AMPERE current maps show there is a clear NBZ current pattern. The NBZ current pattern is the pair of upwards and downwards FACs located at latitudes near 80° latitude or higher on the dayside of the polar cap, with reversed polarity FACs at lower latitudes, associated with the reverse lobe cells (Iijima & Shibaji, 1987; Milan et al., 2020). The currents appear stronger in the northern hemisphere, an asymmetry that

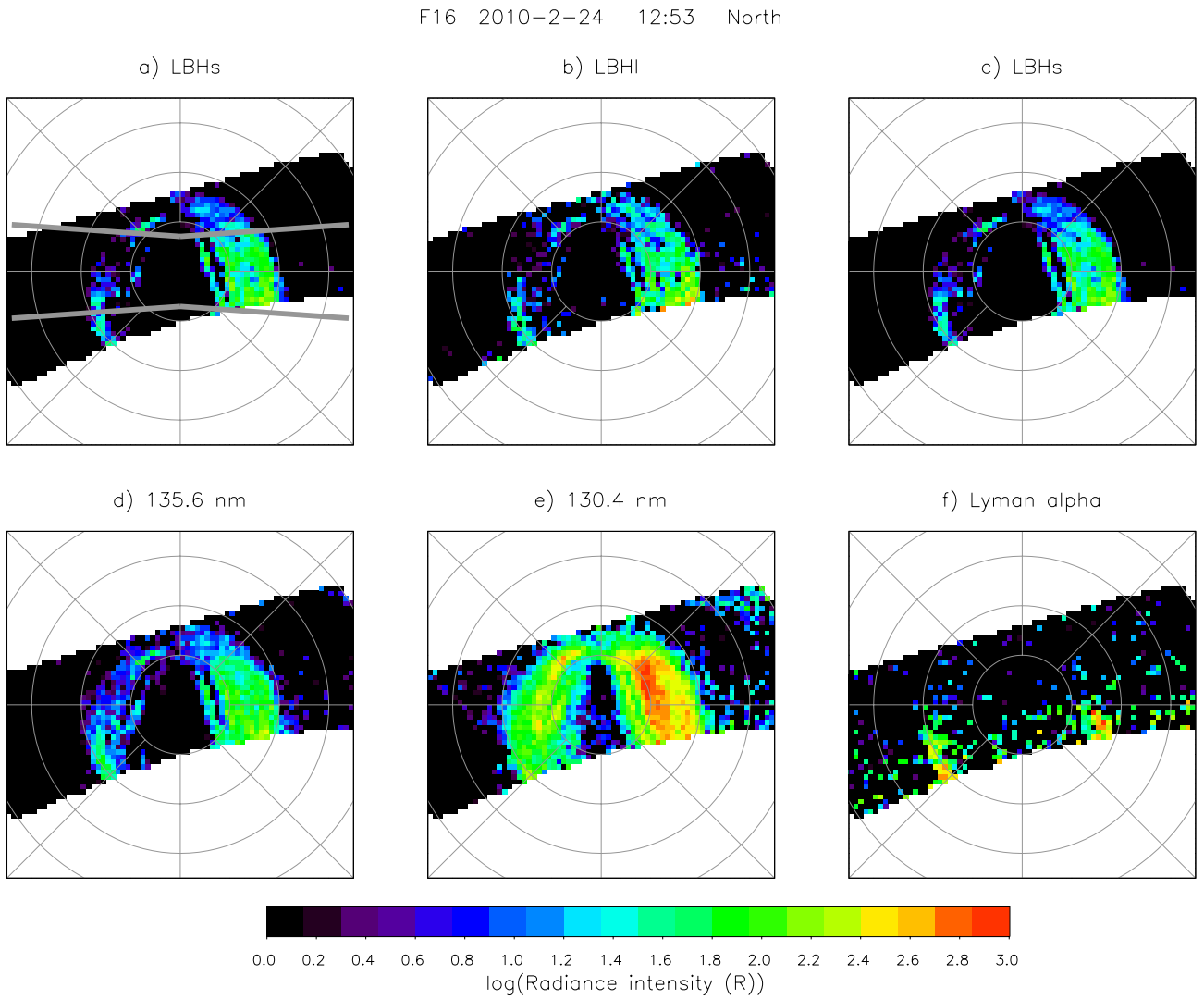

Figure 7. DMSP-F16-SSUSI data from 2010-2-24 12:52 UT in the Northern hemisphere (a) The dusk-dawn radiance intensity averaging area. (b) Example of HCA in 135.6 nm and where only the dawn arc is visible in the other wavelengths on 2010/02/24 at 12:52 UT in the northern hemisphere.

was previously noted by Coxon et al. (2016) who suggested this could be an effect of asymmetry in the Earth's magnetic field or in the total electron content in the two hemispheres.

The average intensity of the HCA in the LBHs band is investigated by taking a section of the DMSP/SSUSI image as shown in Figure 7a and averaging vertically in the image space to give an estimate of the average intensity radiance across the dusk-dawn meridian. Figure 8a shows the average radiance intensity across the dusk-dawn meridian for the HCA events in black. The red curve in Figure 8a is the same analysis on all the LBHs DMSP/SSUSI images for all the IMF conditions between 2010 and 2016. Comparing the curves in Figure 8a it can be seen that for the HCA events there is a clear shoulder poleward of the main auroral oval (where the HCA arcs are located) and the main oval is contracted to higher latitudes than on average. It can also be seen that the dawn side auroras have a higher average radiance intensity and although this is also true for the whole data set, particularly in the southern hemisphere, the ratio is higher for the HCA events.

We investigated the HCA in more detail to determine how the brightness of the dawn and dusk sectors differed. We found that in the LBHs band in 62% the dawn side is brighter, in 13% the dusk side is brighter and in 24% they were approximately equal.

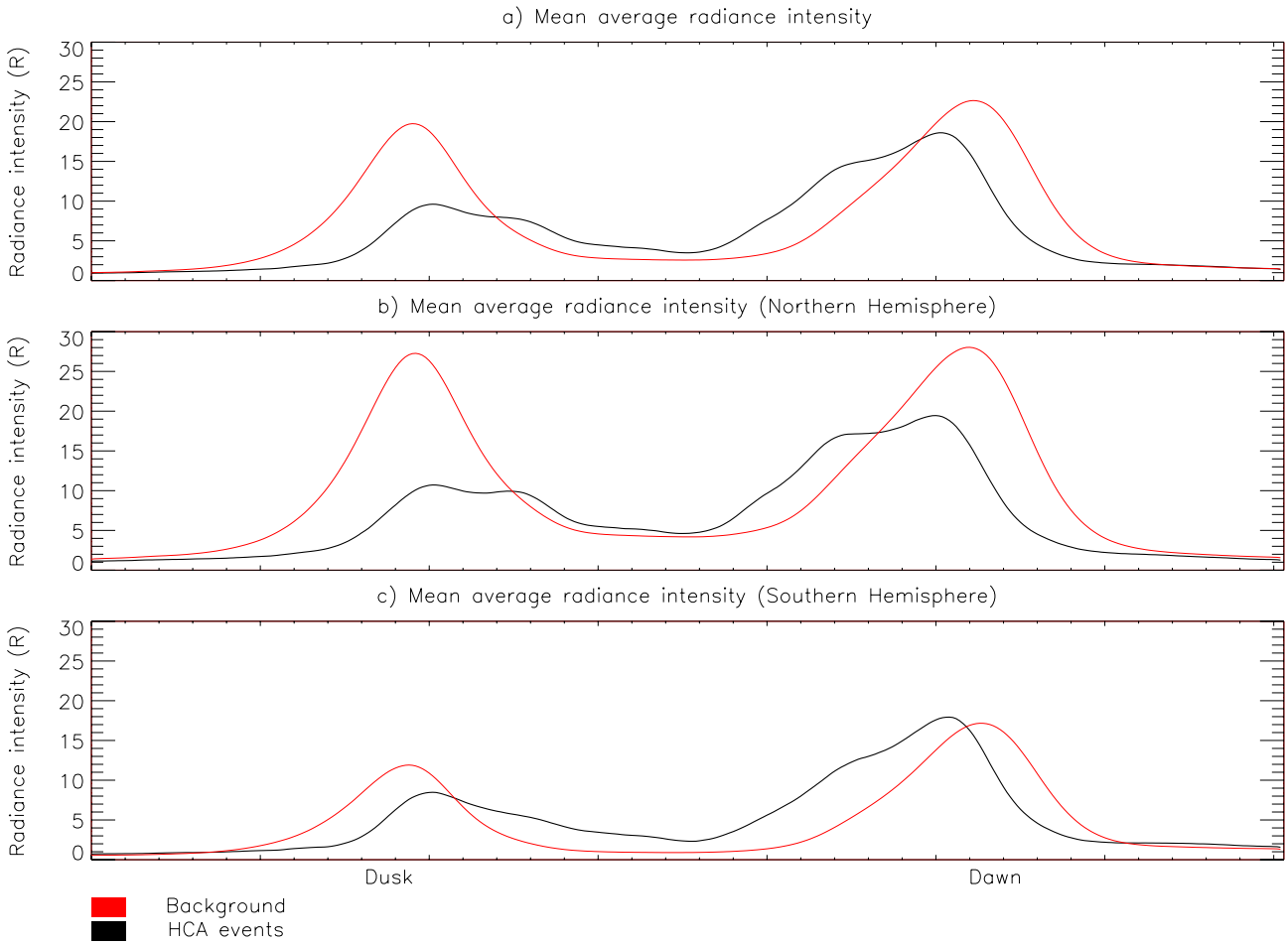

Figure 8. Mean average radiance intensity. (a) Both hemispheres (b) northern hemisphere (c) southern hemisphere black) HCA events red) background.

Figures 8b and 8c show the same analysis but for the northern and southern hemispheres separately. The overall pattern is the same, with brightness being greatest at dawn in both hemispheres, but with the shoulders being more prominent in the northern hemisphere than the southern, although the southern does have a widening of the peak still.

3. Discussion

3.1. Occurrence Statistics

There are 642 HCA events identified in the DMSP/SSUSI data from spacecraft F16, F17 and F18 between January 2010 and December 2016. As seen in Figures 2a and 2c respectively on average there are 8 ± 3 HCA events per month and 92 ± 17 HCA events per year. There is no clear seasonal or solar cycle variation in the occurrence. Each month has a differing number of HCA events per year with the maximum range, the difference between the maximum and minimum number of events in that month, being 7 HCA events. When the standard deviation is considered the majority of the events fall within one standard deviation. The UT distribution (Figure 2b) is explained by the orbit of the DMSP spacecraft and the area scanned by DMSP/SSUSI. As shown in Figures 9d–9f of Bower et al. (2022) less of the central polar cap is scanned at certain UTs in both hemispheres, with approximately 22 to 8 UT in the northern and approximately 0–8 UT in the southern hemisphere not being scanned with enough coverage over the central polar cap. This bias is most prominent in the southern hemisphere. There are also fewer HCA observations between 17 and 22 UT which can be linked to the F18 observations as there are less

HCA identified in the F18 observations and it has poorer coverage in the northern hemisphere compared to the other spacecraft (Bower et al., 2022).

Out of the 642 HCA events 435 of them are made up of multiple DMSP/SSUSI images allowing an estimate of the duration of the HCA to be calculated taking the first DMSP/SSUSI image of the HCA event as the start time and the last as the end time. The HCA events seen only in one DMSP/SSUSI image maybe due to the HCA interval being too short to be seen in multiple images. The DMSP spacecraft are all in approximately 100 minute orbits. Assuming the HCA should be visible in both hemispheres the time between images is ∼50 min for each spacecraft; however as we have used three DMSP spacecraft this separation can be shorter. The mean duration of the HCA events is found to be 2.29 hr and the median to be 1.70 hr. This median is close to the 100 min orbit of the spacecraft. Figure 2e shows the occurrence distribution of duration in 30 min bins and it can bee seen that the majority of the HCA events occur for shorter durations. It is therefore likely that these single image HCA events are shorter events.

The IMF conditions averaged during the hour before the start of the HCA event are as expected, positive (northward) for the IMF B_z component (Figure 3c) with a small average θ (Figure 3d). This is supported by the KS test result where the hull hypnosis that the background and HCA events occur under the same conditions is rejected for IMF B_z and θ but not for the other IMF parameters (B_x, B_y, N_{sw} and V_{sw}), therefore it is clear that the HCA form when the IMF B_z is positive and θ small.

As shown in Figure 3d θ is smaller for HCA events than for the average solar wind conditions of 2010-2016. Imber et al. (2006) suggested that the θ should be below $\pm 10°$ for DLR to occur. For the HCA events identified here, the θ reduces to a mean of approximately $-3.17°$ in the hour before the start of the HCA event (the first DMSP/SSUSI image of the event) with a mean resultant length of 0.77. The criterion is not as stringent as that identified by Imber et al. (2006), but it is clear that near-zero clock angle is required for DLR to occur. 50% of the events have a clock angle of between $-33°$ and $25°$ in the hour before the event; this spread could be due to the uncertainty of the start time of the HCA events as discussed earlier in regard to the duration of the HCA events. The mean length of time the θ stays below $20°$ in the hour before the first image in an HCA event is approximately 9 min (Figure 5b).

The factors that govern the occurrence and rate of lobe reconnection are unclear. It has been suggested in the past that lobe reconnection should be favored in the summer hemisphere, and that positive or negative IMF B_x favors the southern or northern hemispheres, respectively (Lockwood & Moen, 1999). We might expect to see this reflected in our seasonal and IMF B_x distributions. For instance, if lobe reconnection is disfavored in the winter hemisphere, we might expect to see reductions in the occurrence of HCA around June (winter solstice in the southern hemisphere) and December (winter solstice in the northern hemisphere). There is a slight dip around June and July, but this does not seem significant with a chi-squared test p-value of 0.9218. We might also expect $B_x > 0$ to be disfavored in northern winter (December) and $B_x < 0$ disfavored in southern winter (June) for lobe reconnection resulting in fewer observed HCAs. However, Figure 4a shows the B_x distribution for May, June, and July (red) and November, December, and January (blue) and there is no difference in the two distributions. This is supported by a KS test statistic of 0.1330 and a rejection threshold of 0.2302 at a significant level of 0.01.

The equinoxes (Figure 4b) however are statistically different based on a KS test statistic of 0.4310 and a rejection threshold of 0.2302 at a significance level of 0.01. Initial inspection of the equinoxes shows a preference for the HCA to form under positive (negative) B_x in the autumn (spring) however this is explained by the coordinate system used. The IMF data is in GSM coordinates, which are fixed to the magnetic axis of the Earth. Figure 9 shows the difference in the IMF clock angle distributions for the equinox and solstice months of 2010 to 2016 in the GSM and GSE coordinate systems. The difference between GSE and GSM coordinate systems is more pronounced at the equinoxes than the solstices. For June and December the distributions are very similar in GSE and GSM. However during September the GSM data is inclined such that under northward IMF, and therefore during the formation of HCA, GSM B_y is more likely to be negative. The opposite is true in March, such that GSM B_y is more likely to be positive. Therefore during autumn the axis of the Earth is tilted so that under GSM coordinates IMF B_y is more likely to be negative. Under a typical Parker spiral $B_x \approx -B_y$ (Parker, 1958), therefore we except B_x to be positive, as seen, with the opposite being true in spring. This is supported by the IMF B_y distribution (not shown) where in autumn (spring) IMF B_y is negative (positive) for the HCA events. Therefore this suggests that B_x is not an important factor in determining the occurrence of HCA.

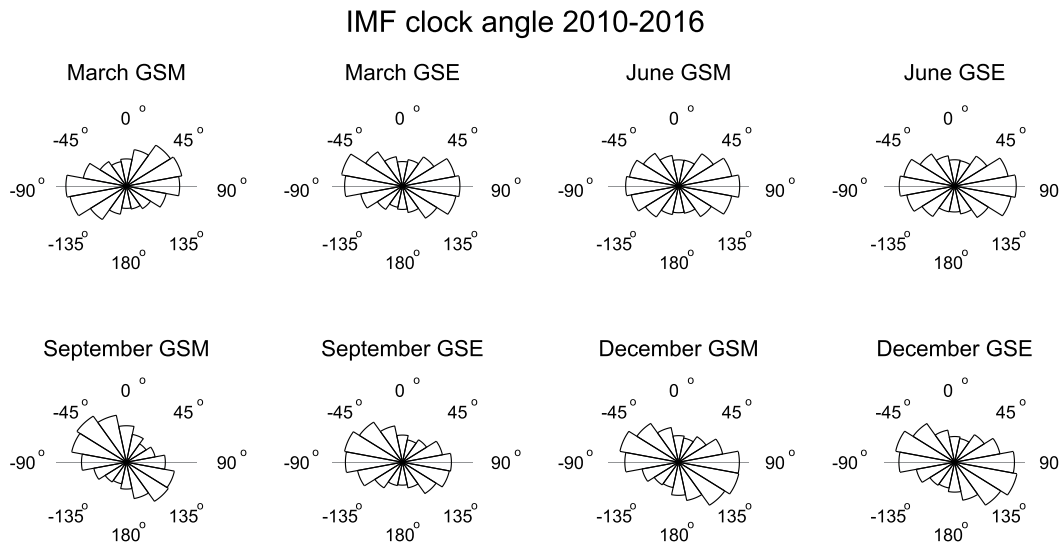

Figure 9. IMF clock angle between 2010 and 2016 in GSE and GSM coordinate systems for equinox months (March and September) and Solstice months (June and December). The gray horizontal line is to help guide the eye between northward and southward IMF.

3.2. HCA Morphology and Relation to TPAs

The mean of the average radiance intensity in the LBHs band across the dusk-dawn meridian shows the HCA has a clear shoulder on the inside of the auroral oval and that the dawn emission is usually brighter (Figure 8). We suggest that the dawn arc of the HCA is bright due to the field aligned current pattern. Milan et al. (2020) Figure 3i shows a schematic of the expected polarity of the field aligned currents during HCA in the Milan et al. (2020) model. The red represents the upward current and the blue the downward current. The dawn arc of the HCA is collocated with the upward current and therefore downward going electrons that are more likely to create electron aurora. As such we would expect the dawn arc to be brighter in the LBHs band as it is primarily measuring electron aurora.

The dawn/dusk asymmetry of the HCA emission brightness perhaps resolves a long-standing problem in understanding the auroral configuration during northward IMF. Bower et al. (2022) undertook an automated search for transpolar arcs (TPAs) in SSUSI data and found a preponderance of TPAs at dawn as opposed to dusk; they also noted that such an asymmetry had been recorded in previous studies (Fear & Milan, 2012; Hosokawa et al., 2011; Rairden & Mende, 1989). We now propose that HCAs with sufficiently dim dusk emission could be misidentified as a lone TPA at dawn. We now reassess the TPA occurrence from the event list of Bower et al. (2022).

From the TPA list obtained in Bower et al. (2022) the TPAs seen in both hemispheres simultaneously have been plotted based on their location across the dusk-dawn meridian in degrees of colatitude. Figure 10a shows the average location of the TPA across the dusk-dawn meridan during the lifetime of the TPA with error bars. The error comes from the detection algorithm used to identify the TPAs, in which there is an uncertainty of ±4.8° colatitude on the location of the arc. The observations fall into three main groupings: dawn in the northern hemisphere and dusk in the southern hemisphere, dusk in the northern hemisphere and dawn in the southern hemisphere, and dawn in both northern and southern hemispheres. The dawn-dusk quadrants have been shaded in green and the dawn-dawn quadrant in yellow. The green quadrants are consistent with the expectation that TPAs in the northern hemisphere will form at dusk or dawn if IMF B_y is positive or negative, respectively, with the opposite behavior in the southern hemisphere (Fear & Milan, 2012; Milan et al., 2005). There are roughly similar numbers of events in the two green quadrants. The yellow quadrant accounts for the preponderance of dawn TPAs reported by Bower et al. (2022) and others (Hosokawa et al., 2011; Rairden & Mende, 1989; Valladares et al., 1994). These we suspect are misidentified HCA, which we test below. The red triangles in Figure 10a are HCA identified in the present study that were originally included in the TPA list.

Figures 10b and 10c show the start location of the arcs and are color coded based on the IMF B_y and B_z components in the 3–4 hr before the first DMSP/SSUSI image respectively. 3–4 hr before the event was chosen as it

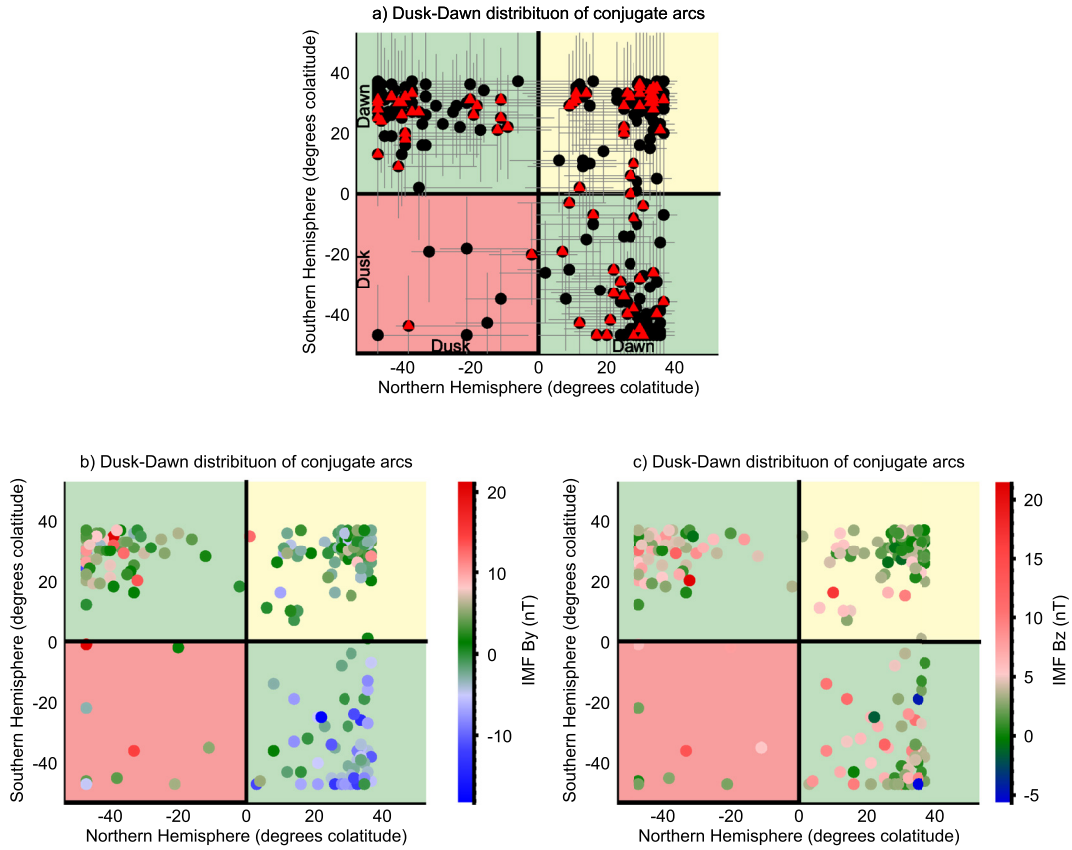

Figure 10. (a) Average location of conjugate TPA event across the dusk dawn meridian with error bars. Red triangle points are events that are classified as HCA here. Start location of TPA event color coded based on the IMF conditions in the 3–4 hr before the events start time. (b) B_y (c) B_z.

have previously been shown by Fear and Milan (2012) that this is the time period that has the most effect on the location of formation of TPAs. The error bars have been removed for clarity. As can be seen from Figure 10c the vast majority of arcs are observed for $B_z > 0$, as expected. The arcs in that occur at dawn in both hemispheres also appear to form when the IMF B_z is closer to zero then the arc that form at dusk in one hemisphere and dawn in the other which appear to form when the IMF B_z component is stronger.

The dusk-dawn arcs, arcs that occur at dusk in the northern hemisphere and dawn in the southern hemisphere, occur mainly when IMF B_y is positive, with dawn-dusk arcs occurring when the IMF B_y is negative. This is in agreement with the findings of Fear and Milan (2012) who showed that in the southern hemisphere TPAs are more likely to form at dawn if IMF B_y is positive in the 3–4 hr before the event, and more likely to form at dusk if negative. Similarly in the northern hemisphere more TPAs are likely to form at dawn if the IMF B_y in the 3–4 hr before the event is negative and more likely to form at dusk if positive. This observation is consistent with the Milan et al. (2005) model of TPA formation.

The dawn-dawn arcs however occur most often when B_y is closer to zero. Some uncertainties are expected in the timing between the onset of HCA/TPA and the relevant solar wind measurements due to the relatively poor cadence of the DMSP observations.

We inspected the DMSP/SSUSI images that make up the dawn-dawn arcs. We found that a significant number were originally misclassified as TPA when in fact they are HCA with a brighter dawn arc than dusk arc (consistent with the average seen in Figure 8). Some of these are missing from the list of HCA identified between Jan 2010 and Dec 2016 as they are clear in the 135.6 nm and not the 130.nm or the LBHs which were used to identify the HCA. Figure 7b shows an example of this for 2010/02/24 at 12:52 UT in the northern hemisphere. In Figure 7b (ii) and iii) it can also be seen that only the dawn arc is visible in the LBHs and the 130.nm. We

suggest that there are a large proportion HCA where the dawn arc is brighter than the dusk and as such are easily misclassified as a TPA. Of the dawn-dawn arcs 46% are HCA with a further 36% being possible HCA where the dawn arc is brighter. 15% are misclassified as dawn-dawn TPAs and fall in to the dawn-dusk or dusk-dawn boxes when the error on their location is considered. The final 3% appear to be actual dawn-dawn arcs. The detection algorithm used to identify the TPAs works by identifying the peak in average radiance intensity above 12.5° colatitude and as such will always identify the location based on the brightest arc which in the case of the HCA is usually the dawn arc. The HCA events studied by Sharber et al. (1992) supports this. Their event which occurred on 2nd December 1981 and was imaged between 14:21 and 15:46 UT by DE-1 first clearly showed the well-defined dawnside web and arc feature with the duskside not being clear until 15:10 UT, although they note that the general pattern is present throughout the period. Thus we suggest that the dawn-dawn TPAs are actually HCA where the dawn arc is brighter due to being colocated with a region of upward FAC. A similar preponderance of dawnside TPAs has been identified by previous authors (Hosokawa et al., 2011; Rairden & Mende, 1989; Valladares et al., 1994), and this could similarly explain their results.

4. Conclusion

642 horse collar auroras (HCA) events were identified in the DMSP/SSUSI data between January 2010 and December 2016. There is no clear seasonal or UT dependence that cannot be attributed to the restrictions of the DMSP/SSUSI data. On average, there are 8 HCA events per month and 92 events per year. HCA occur under northward IMF when θ is small between −33° and 25° in the hour before the HCA events. There is no correlation between IMF B_x, B_y, solar wind density or solar wind speed with the occurrence of HCA. It has long been thought that IMF B_x will play a role in modulating lobe reconnection, either favoring or disfavoring reconnection in the winter hemisphere. Our results suggest that B_x is not an important factor in determining the occurrence of HCA. $|\theta|$ reduces in the 4 hr before the HCA events, reaching a mean of −3.17° in the hour before the start of the HCA event with a mean resultant length of 0.77. In the hour before the HCA the average θ stays below 20° for an average of 9 min. The HCA events have an average duration of 2.29 hr, the accuracy of which is limited by the cadence of the DMSP/SSUSI images.

The HCA events show a clear shoulder in the average radiance intensity poleward of the main auroral oval and the main oval is contracted toward the poles more than average when compared to all the DMSP/SSUSI images in 2012. It can also be seen that the dawn side arc has a higher average radiance intensity and although this is also true for all the 2012 DMSP/SSUSI images, the ratio is higher for the HCA images. This can be explained using the Milan et al. (2020) model and the expected FAC during the HCA. As the upward current is collocated with the dawn arc of the HCA we would expect the dawn arc to be brighter in the LBHs band as seen, as it is primarily measuring electron aurora. That the dawnside arc tends to be brighter than the duskside arc perhaps explains the preponderance of transpolar arcs identified simultaneously in the dawn sector in both hemispheres in previous studies.

It should also be possible to verify the HCA identified in the DMSP/SSUSI data with the use of SuperDARN flow maps to check for sunward ionospheric flows across the polar cap. Understanding HCA statistics will allow DLR to be studied in more detail. HCA should also be magnetically connected to regions of dense plasma within the magnetosphere, captured from the solar wind so there is further work to be done looking at in situ spacecraft data to verify this.

Data Availability Statement

The DMSP/SSUSI file type EDR-AUR data were obtained from http://ssusi.jhuapl.edu (data version 0106, software version 7.0.0, calibration period version E0018). AMPERE data were obtained from http://ampere.jhuapl.edu.

Acknowledgments
GEB is supported by a Science and Technology Facilities Council (STFC), UK, studentship. SEM is supported by STFC grant no. ST/S000429/1. The work at the Birkeland Centre for Space Science is supported by the Research Council of Norway under contract 223252/F50. The authors acknowledge use of NASA/GSFC's Space Physics Data Facility's CDAWeb service and OMNI data (at http://cdaweb.gsfc.nasa.gov).

References

Anderson, B. J., Takahashi, K., & Toth, B. A. (2000). Sensing global birkeland currents with iridium® engineering magnetometer data. *Geophysical Research Letters*, *27*(24), 4045–4048. https://doi.org/10.1029/2000GL000094

Bower, G. E., Milan, S. E., Paxton, L. J., & Imber, S. M. (2022). Transpolar arcs: Seasonal dependence identified by an automated detection algorithm. *Journal of Geophysical Research: Space Physics*, *127*, e2021JA029743. https://doi.org/10.1029/2021JA029743

Carter, J. A., Milan, S. E., Fogg, A. R., Paxton, L. J., & Anderson, B. J. (2018). The association of high-latitude dayside aurora with nbz field-aligned currents. *Journal of Geophysical Research: Space Physics*, *123*(5), 3637–3645. https://doi.org/10.1029/2017JA025082

Coxon, J. C., Milan, S. E., & Anderson, B. J. (2018). A Review of Birkeland Current Research Using AMPERE. *A review of birkeland current research using ampere. Electric currents in geospace and beyond*, 257–278. https://doi.org/10.1002/9781119324522.ch16

Coxon, J. C., Milan, S. E., Carter, J. A., Clausen, L. B. N., Anderson, B. J., & Korth, H. (2016). Seasonal and diurnal variations in ampere observations of the birkeland currents compared to modeled results. *Journal of Geophysical Research: Space Physics*, *121*, 4027–4040. https://doi.org/10.1002/2015JA022050

Fear, R. C., & Milan, S. E. (2012). The IMF dependence of the local time of transpolar arcs: Implications for formation mechanism. *Journal of Geophysical Research*, *117*. https://doi.org/10.1029/2011JA017209

Frey, H. U. (2007). Localized aurora beyond the auroral oval. *Reviews of Geophysics*, *45*(1). https://doi.org/10.1029/2005RG000174

Hones, E. W., Craven, J. D., Frank, L. A., Evans, D. S., & Newell, P. T. (1989). The horse-collar aurora: A frequent pattern of the aurora in quiet times. *Geophysical Research Letters*, *16*(1), 37–40. https://doi.org/10.1029/GL016i001p00037

Hosokawa, K., Kullen, A., Milan, S., Reidy, J., Zou, Y., Frey, H. U. R. M., et al. (2020). Aurora in the polar cap: A review. *Space Science Reviews*, *216*(1), 1–44. https://doi.org/10.1007/s11214-020-0637-3

Hosokawa, K., Moen, J. I., Shiokawa, K., & Otsuka, Y. (2011). Motion of polar cap arcs. *Journal of Geophysical Research*, *116*(A1). https://doi.org/10.1029/2010JA015906

Iijima, T., & Shibaji, T. (1987). Global characteristics of northward imf-associated (nbz) field-aligned currents. *Journal of Geophysical Research*, *92*(A3), 2408–2424. https://doi.org/10.1029/JA092iA03p02408

Imber, S. M., Milan, S. E., & Hubert, B. (2006). The auroral and ionospheric flow signatures of dual lobe reconnection. *Annals of Geophysics*. https://doi.org/10.5194/angeo-24-3115-2006

King, J. H., & Papitashvili, N. E. (2005). Solar wind spatial scales in and comparisons of hourly wind and ace plasma and magnetic field data. *Journal of Geophysical Research*, *110*(A2). https://doi.org/10.1029/2004JA010649

Lockwood, M., & Moen, J. (1999). Reconfiguration and closure of lobe flux by reconnection during northward imf: Possible evidence for signatures in cusp/cleft auroral emissions. *Annales Geophysicae*, *17*, 996–1011. https://doi.org/10.1007/s00585-999-0996-2

Mardia, K. V., & Jupp, P. E. (2009). *Directional statistics*. John Wiley & Sons.

Meng, C.-I. (1981). Polar cap arcs and the plasma sheet. *Geophysical Research Letters*, *8*(3), 273–276. https://doi.org/10.1029/GL008i003p00273

Milan, S. E., Bower, G. E., Carter, J. A., Paxton, L. J., Anderson, B. J., & Hairston, M. R. (2022). Dual-lobe reconnection and cusp-aligned auroral arcs. *Journal of Geophysical Research: Space Physics*.

Milan, S. E., Carter, J. A., Bower, G. E., Imber, S. M., Paxton, L. J., Anderson, B. J., et al. (2020). Dual-lobe reconnection and horse-collar auroras. *Journal of Geophysical Research: Space Physics*, *125*(10), e2020JA028567. https://doi.org/10.1029/2020JA028567

Milan, S. E., Hubert, B., & Grocott, A. (2005). Formation and motion of a transpolar arc in response to dayside and nightside reconnection. *Journal of Geophysical Research: Space Physics*, *110*(A1). https://doi.org/10.1029/2004JA010835

Parker, E. N. (1958). Dynamics of the interplanetary gas and magnetic fields. *The Astrophysical Journal*, *128*, 664. https://doi.org/10.1086/146579

Paxton, L. J., Meng, C.-I., Fountain, G. H., Ogorzalek, B. S., Darlington, E. H., Gary, S. A., et al. (1992). Special sensor ultraviolet spectrographic imager: An instrument description. *Instrumentation for planetary and terrestrial atmospheric remote sensing*. International Society for Optics and Photonics. https://doi.org/10.1117/12.60595

Paxton, L. J., Meng, C.-I., Fountain, G. H., Ogorzalek, B. S., Darlington, E. H., Gary, S. A., et al. (1993). Ssusi: Horizon-to-horizon and limb-viewing spectrographic imager for remote sensing of environmental parameters. *Ultraviolet technology IV*. International Society for Optics and Photonics. https://doi.org/10.1117/12.140846

Paxton, L. J., Schaefer, R. K., Zhang, Y., & Kil, H. (2017). Far ultraviolet instrument technology. *Journal of Geophysical Research: Space Physics*, *122*(2), 2706–2733. https://doi.org/10.1002/2016JA023578

Paxton, L. J., & Zhang, Y. (2016). *Far ultraviolet imaging of the aurora*. Space weather fundamentals.

Rairden, R. L., & Mende, S. B. (1989). Properties of 6300-å auroral emissions at south pole. *Journal of Geophysical Research*, *94*(A2), 1402–1416. https://doi.org/10.1029/JA094iA02p01402

Sharber, J. R., Hones, E. W., Jr., Heelis, R. A., Craven, J. D., Frank, L. A., Maynard, N. C., et al. (1992). Dynamics explorer measurements of particles, fields, and plasma drifts over a horse-collar auroral pattern. *Journal of Geomagnetism and Geoelectricity*, *44*(12), 1225–1237. https://doi.org/10.5636/jgg.44.1225

Tanaka, T., Obara, T., Watanabe, M., Fujita, S., Ebihara, Y., & Kataoka, R. (2017). Formation of the sun-aligned arc region and the void (polar slot) under the null-separator structure. *Journal of Geophysical Research: Space Physics*, *122*(4), 4102–4116. https://doi.org/10.1002/2016JA023584

Valladares, C. E., Carlson, H. C., Jr., & Fukui, K. (1994). Interplanetary magnetic field dependency of stable sun-aligned polar cap arcs. *Journal of Geophysical Research*, *99*(A4), 6247–6272. https://doi.org/10.1029/93JA03255

Waters, C. L., Anderson, B. J., & Liou, K. (2001). Estimation of global field aligned currents using the iridium® system magnetometer data. *Geophysical Research Letters*, *28*(11), 2165–2168. https://doi.org/10.1029/2000GL012725